



# CHORUS

This is the accepted manuscript made available via CHORUS. The article has been published as:

## Rare-region onset of superconductivity in niobium nanoislands

Malcolm Durkin, Rita Garrido-Menacho, Sarang Gopalakrishnan, Narendra K. Jaggi, Ji-Hwan Kwon, Jian-Min Zuo, and Nadya Mason

Phys. Rev. B **101**, 035409 — Published 10 January 2020

DOI: [10.1103/PhysRevB.101.035409](https://doi.org/10.1103/PhysRevB.101.035409)

1 **Rare-region onset of superconductivity in Niobium nano-islands**

2 Malcolm Durkin<sup>1</sup>, Rita Garrido-Menacho<sup>1</sup>, Sarang Gopalakrishnan<sup>2</sup>, Narendra K Jaggi<sup>3</sup>, Ji-Hwan Kwon<sup>4</sup>,  
3 Jian-Min Zuo<sup>4</sup>, and Nadya Mason<sup>1</sup>

4 <sup>1</sup>*Department of Physics and Frederick Seitz Materials Research Laboratory, University of Illinois at*  
5 *Urbana-Champaign, Urbana IL 61801, USA*

6 <sup>2</sup>*Department of Engineering Science and Physics, College of Staten Island, Staten Island NY 10314, and*  
7 *Initiative for the Theoretical Sciences, CUNY Graduate Center, New York NY 10016, USA*

8 <sup>3</sup>*Department of Physics, Illinois Wesleyan University, Bloomington, IL 61702, USA*

9 <sup>4</sup>*Department of Materials Science and Frederick Seitz Materials Research Laboratory, University of*  
10 *Illinois at Urbana-Champaign, Urbana IL 61801, USA*

11  
12 We report measurements of the superconducting properties of isolated Nb nano-islands (600 nm -  
13 2500 nm diameters) and explain their unusual behavior in terms of rare-region onset effects, predicted for  
14 random metal-superconductor granular systems [B. Spivak, P. Oredo, S. A. Kivelson, Phys. Rev. B **77**,  
15 214523 (2008)]. We find that the island  $T_c$  is strongly suppressed even at large island diameters,  
16 exceeding 1  $\mu\text{m}$ . This behavior is unexpected given that conventional theories of superconductivity in  
17 small grains predict suppression of  $T_c$  only at a length scale that is two orders of magnitude smaller. In  
18 addition, we observe large island-to-island variations in  $T_c$  for nominally identical islands. These two  
19 experimental observations, coupled with direct measurement of grain distribution using TEM, conductive  
20 AFM, and computer simulations, provide evidence for our picture in which the onset of superconductivity  
21 on an island coincides with the transition temperature of its largest constituent grain, and then spreads to  
22 other grains due to proximity coupling.

23 **I. INTRODUCTION**

24 An ongoing question in physics is: What determines the critical behavior of disordered systems?  
25 Recent evidence has suggested that many disordered systems—from metals [1] to magnets [2] to a wide  
26 variety of superconductors [3,4,5,6,7,8,9] might be dominated by the behavior of “rare-regions” of a  
27 correlated phase, which control the inception and dynamics of bulk electronic phases. Disorder is present  
28 at the microscopic level in all physical systems. In typical three-dimensional systems, this microscopic  
29 disorder averages out when computing macroscopic, long-wavelength response properties. However, in

30 many low-dimensional correlated phases of matter, even moderate microscopic disorder can have drastic  
31 implications for macroscopic transport: examples include Anderson localization even in the presence of  
32 weak disorder in one or two dimensions [10], 2D quantum metals [3,5,9,11], quantum Griffiths phases  
33 [7], and related states. In many of these examples, disorder does not “self-average” on large scales: the  
34 large-scale properties of the material are determined, not by its *typical* parameter values, but by regions  
35 with anomalous parameters (i.e., “rare-regions”) that have an outsize effect on response. Experimentally,  
36 rare-region effects are often inferred from macroscopic measurements; experimentally identifying the  
37 microscopic spatial distributions of local parameters has only been feasible in a few cases.

38 The superconductor-metal-insulator transition in disordered superconducting thin films is  
39 believed to exhibit strong rare-region effects. In superconducting thin films, increasing disorder is  
40 predicted to generate a continuous quantum phase transition between a superconducting and insulating  
41 state, as the normal state resistance (a proxy of disorder) approaches the quantum of resistance ( $R_Q \sim 6.4$   
42  $k\Omega$ ) [12]. However, multiple experiments have instead demonstrated that superconductivity is suppressed  
43 at much lower values of the film resistance and phase transitions to low-resistance metals [11,13,14]. The  
44 main theoretical paradigm for understanding such superconductor-metal-insulator transitions [3,4,5]  
45 assumes that the films possess emergent inhomogeneity, i.e., they break up into locally superconducting  
46 islands in a metallic matrix.

47 While early quantitative studies of inhomogeneous superconductors focused on percolating  
48 networks of weakly-coupled superconducting grains embedded in non-metallic matrices [15,16], very  
49 low-resistance granular films, where superconducting grains are embedded in a metal, have not been well-  
50 studied experimentally, and a direct connection with pertinent theoretical work [3] has not been  
51 attempted. In the well-coupled regime, randomness in grain size dominates, and global superconductivity  
52 appears rapidly after the transition of the largest superconducting grain (i.e., a “rare-region”). This type of  
53 low-resistance, highly inhomogeneous superconductivity has been invoked to explain many recent  
54 experimental results [6,7,8,9,17], and rare superconducting domains have been observed above the  
55 superconducting transition in NbN [18]. However, these works did not connect the observed behavior to  
56 the distribution of grains, or to any specific theory of rare-region onset of superconductivity.

57 In previous work [19], we studied arrays of Nb islands on Au films, finding anomalous island  $T_c$   
58 dependence on the strength of coupling between islands. In this paper, we present measurements

59 performed on individual islands, eliminating the coupling between islands. We find that the  $T_c$  of these  
60 islands is strongly suppressed, even for island diameters of over 1200 nm, diameters much larger than the  
61 260 nm that had been used in our previous study of island arrays. This behavior is unexpected given that  
62 conventional theories of superconductivity in small grains [20] predict suppression of  $T_c$  only at a length  
63 scale that is two orders of magnitude smaller, which is consistent with previous experiments on isolated  
64 superconducting grains [21,22,23]. In addition, we observe strong island-to-island fluctuations of  $T_c$  for a  
65 broad range of island diameters. This paper presents data for the temperature dependent resistance,  $R(T)$ ,  
66 of a broad range of islands and their detailed materials characterization, especially a direct measurement  
67 of the grain-size distribution using conductive Atomic Force Microscopy (c-AFM). Guided by Spivak *et*  
68 *al* [3], we use a combination of experimental results and computer simulations to provide a picture for the  
69 emergence of superconductivity in this system using the concept of rare-region onset.

70

## II. EXPERIMENTAL METHODS

71 Islands were composed of 70 nm thick electron-beam evaporated Nb, on top of insulating SiO<sub>2</sub>  
72 substrates, and had diameters varying between 600 nm and 2500 nm [Fig. 1(a)]. Nb was chosen because it  
73 forms nanoscale grains when either sputtered or evaporated, with structure and grain size dependent on  
74 deposition parameters [24]. We patterned our samples using electron beam lithography on PMMA,  
75 electron beam evaporation, and liftoff processes all on a silicon wafer with a 300 nm oxide layer. We first  
76 made the four-point contacts, which consist of 1 nm of Ti and 10 nm of Au. Then we patterned a Nb  
77 island on top of the normal metal contacts. Nb was deposited in an ultra-high vacuum (UHV) system with  
78 a 67 cm throw distance. A brief ion-mill was performed prior to electron beam evaporating 70 nm of Nb  
79 at a pressure of  $1.0 \times 10^{-9}$  Torr or less. The Au contacts had a 50-100 nm overlap underneath the Nb island.  
80 The sample was then placed in a chip carrier, contacted with a wedge bonder, and measured in a 1K  
81 cryostat using standard lock-in amplifier techniques.

82

## III. EXPERIMENTAL MEASUREMENTS

83 We measured  $R(T)$  for scores of islands, of varying diameters. Each panel in Fig. 1(b-h) shows  
84  $R(T)$  for approximately ten islands, all having the same thickness, the same diameter, and grown on the  
85 same chip, under identical conditions, and measured in the same run. While each island has a well-  
86 defined and stable (reproducible) “onset” temperature, as indicated by the sudden decrease in resistance,  
87 this onset temperature is different for different islands of nominally the same diameter. For example, for

88 the set of islands with a diameter of 600 nm, the onset  $T_c$  varies from 2.6 K to 5.1 K, even though their  
89 thickness and diameter are within a few percent of each other. The amount of this unusually large island-  
90 to-island variation of the onset  $T_c$  decreases as the diameter increases, but it clearly persists at least up to a  
91 diameter of 1400 nm, as shown in the other panels of Fig. 1. This data suggests that the onset behavior of  
92 each island might be dominated by some specific and frozen nanoscale feature of that particular island, a  
93 feature that is at a scale much less than that of the island diameter.

94 To show the important and reproducible observed trends for the superconducting transitions in  
95 this system, we have summarized in Fig. 2 data for seven sets of samples that were prepared under  
96 slightly different evaporation conditions. Each evaporation run evaluated, measured 5 to 12 islands of the  
97 same diameter, (except for E1-E3 where only one island per diameter was evaluated). Fig. 2(a) shows the  
98 dependence of the mean  $T_c$  upon the diameter of the island. The curves all show the same qualitative  
99 behavior:  $T_c$  is strongly suppressed as diameter is decreased below  $\sim 1 \mu\text{m}$ . For large islands ( $> 2 \mu\text{m}$ ),  $T_c$   
100 approaches the bulk value for Nb, 9.1 K. However, as the island diameter is decreased,  $T_c$  drops sharply,  
101 to below 4 K at  $1 \mu\text{m}$ , and well below that for smaller diameters. To summarize the observed behavior of  
102 island-to-island fluctuations, we show in Fig. 2(b) the standard deviation of  $T_c$  versus the corresponding  
103 mean value of  $T_c$  for four sets of samples (E4-E7) for which 5 to 12 islands of the same diameter were  
104 measured. Over the range of diameters explored in this study, these island-to-island fluctuations increase  
105 as island diameter decreases.

106 The set labelled E2 Au in Fig. 2 shows that data for islands on gold squares is nearly identical to  
107 islands placed on insulators as shown by sets E1-E7. This demonstrates that the normal metal (either  
108 underlying, or in the leads) is not the reason for suppression of the transition temperature. The micron-  
109 length scales at which superconductivity is suppressed in these islands are far longer than other length  
110 scales related to superconductivity in Nb, such as the coherence length ( $\sim 29 \text{ nm}$ ) [19] or the scale at  
111 which the gap equals the discrete energy level spacing ( $\sim 4 \text{ nm}$ ) [21,24].

112 We note that qualitatively similar size dependence of  $T_c$  in Nb nano-structures and films has been  
113 observed in past works [25,26,27]. They found that submicron niobium structures patterned with ordinary  
114 PMMA resist had a significantly suppressed  $T_c$  compared to the  $T_c$  of co-evaporated Nb structures  
115 patterned using MMA/PMMA, ZEP520A, and ZEP520A with Ti passivation.

116 Because of the technological importance of Nb-based superconducting nanowire single photon  
117 detectors, these size dependence effects are well documented and various fabrication techniques to  
118 improve the  $T_c$  of Nb-nanowires have been explored [25,26,27]. But the underlying physical mechanism  
119 has not been studied previously. In addition, the most interesting experimental features, e.g., the very  
120 large island-to-island fluctuation of  $T_c$  and their systematic dependence on island diameter, have not been  
121 reported in past works. This paper provides comprehensive new data, detailed materials characterization,  
122 and finds semi-quantitative agreement of the data with computer simulations based upon a particular  
123 theory [3]. Altogether it builds an intuitively transparent picture for the emergence of superconductivity in  
124 this system using the concept of rare-region onset.

## 125 IV. DISCUSSION

### 126 A. Materials characterization

#### 127 1. TEM Characterization of grains

128 Figure 3 shows typical transmission electron microscopy (TEM) images of our Nb islands, where  
129 black crystals (the “grains”) are surrounded by gray, amorphous-like material. Top view TEM  
130 measurements were performed on Nb islands placed on TEM windows, which consist of a 20 nm thick  
131 SiO<sub>2</sub> membrane. The horizontal measurements were performed by cutting an island cross-section using a  
132 focused ion beam (FIB) and performing a cross-sectional TEM. The TEM characterization shows that the  
133 grains are columnar in shape, suggesting that one could regard each island as a two-dimensional array of  
134 columnar grains.

135 The grain size statistics were extracted from top view TEM images using an object finder, which  
136 applied a low pass filter for smoothing and then identified grains as areas where the image intensity is  
137 below a threshold. Using Fig. 3(a), which has high contrast regions visible in both light and dark, we  
138 executed the described image processing steps followed by the threshold identification. These image  
139 processing steps are shown and articulated in the figure captions for Fig. 4(a-c). As can be seen in Fig. 5,  
140 analysis of these TEM images showed an *exponential distribution* of grain diameters  $L$ ,  $P(L, \beta) = \beta e^{-\beta L}$   
141 with  $\beta = 0.243 \text{ nm}^{-1}$  giving a mean grain diameter of 4.12 nm.

#### 142 2. Conductive AFM characterization of grains

143 Conductive atomic force microscopy (c-AFM) involves performing contact mode AFM  
144 measurements using a conducting cantilever and dragging the cantilever across a sample as depicted in  
145 Fig. 6(a) inset. The tip is held at a constant bias, the sample is grounded at the other end of the chip, and  
146 the current is measured. Due to the narrow tip, the current measured is sensitive to the conductance near  
147 the tip. A resistor network simulation seen in Fig. 6(a) shows current peaks when the tip is above highly  
148 conductive regions. Fig. 6(b) shows the results of conductive AFM measurements performed on 70 nm  
149 thick Nb films, where a distribution of current peaks is evident. The size of these current peaks was  
150 extracted using an object finder and, as can be seen in Fig. 6(c), corresponds to a distribution of grain  
151 diameters  $L$ ,  $P(L, \beta) = \beta e^{(-\beta L)}$  with  $\beta = 0.122 \text{ nm}^{-1}$  giving a mean grain diameter of 8.2 nm. This  
152 exponential distribution is similar to the exponential distribution of grains found using TEM. These two  
153 results together clearly show that the film consists of highly conductive grains embedded in a second  
154 amorphous-like phase that is *metallic*, with a higher resistivity.

155 While c-AFM and TEM data confirm the *exponential nature of grain size distribution* of the  
156 crystalline Nb grains, there is a discrepancy of approximately a factor of 2 in the mean size of these  
157 crystallites. This discrepancy can be understood by the fact that the c-AFM measures conducting  
158 regions—which may contain small clusters of nearly touching grains—while the TEM measures each  
159 individual grain. In particular, the factor of two discrepancy implies that there are multiple clusters of 2-3  
160 small grains (which is also evident by eye in the TEM data). Because what is pertinent for our analysis is  
161 the size of individual grains, the grain size distribution extracted from TEM data is the most relevant and  
162 is used for the theoretical analysis.

### 163 ***3. Combined AFM, EDX, RBS, TEM and XRD characterization of the amorphous-like material***

164 We characterize the amorphous-like Nb phase in the patterned islands based upon a combined  
165 analysis of AFM, energy dispersive X-ray (EDX), Rutherford backscattering (RBS), TEM and X-ray  
166 diffraction (XRD) data. This data confirms that the amorphous phase is metallic, and that it has a  
167 resistivity much higher than that of crystalline Nb. We have evidence that it is not crystalline Nb-oxide, it  
168 is likely a mixture of amorphous and nano-crystalline Nb phases, and that its formation is related to the  
169 outgassing from the PMMA resist during processing. In this section, we summarize the observations that  
170 lead to the above conclusion.

171 RBS data on patterned films fits quite well to a model consisting of the expected 70 nm Nb film  
172 on a 300 nm SiO<sub>2</sub>/Si substrate, but there are small systematic regions of misfit suggesting the  
173 incorporation of a small amount of some other element into the film. Modifying the model to include any  
174 oxygen within the film makes the RBS fits worse, and we therefore believe that we can rule out any  
175 significant amount of NbO<sub>x</sub>. EDX shows small amounts of carbon, but, as always, it is difficult to tell if  
176 the carbon is incorporated into the film, or if it is a surface contamination.

177 XRD measurements were performed on Nb films which were e-beam evaporated under similar  
178 conditions as our Nb islands. A conventional 2 theta/omega XRD scan as well as glancing XRD scan  
179 were performed on these films and it was found that besides Nb and Si (substrate), no other crystalline  
180 materials were present on the film. The widths of the Nb peaks seen in the XRD spectra gave insight into  
181 the crystalline size. The estimated average crystalline size from the XRD results is about 9.7 nm, which is  
182 qualitatively consistent with the c-AFM measurements. Because the islands are very thin (70 nm  
183 thickness) and small (few hundred nm in diameter), and because the second phase is amorphous, as  
184 shown by TEM, we were unable to unambiguously identify the chemical composition of this second  
185 amorphous-like Nb-based phase using XRD.

186 For the purposes of our theoretical model, all that is necessary is for the second phase to be  
187 metallic; whether it is crystalline or amorphous is not relevant to the theoretical model. That the second  
188 phase is indeed metallic is convincingly demonstrated by c-AFM as discussed previously. Scanning  
189 electron nanodiffraction using TEM [28] [Fig. 7] however does provide evidence that the gray regions in  
190 the TEM images indeed have an amorphous-like character, whereas the dark grains are pure crystalline  
191 Nb.

## 192 **B. Theoretical model of superconducting behavior**

193 The key theoretical idea invoked to explain the superconducting properties of this granular metal-  
194 superconductor system is the following: The temperature  $T_c$  for the onset of superconductivity in any  
195 particular island coincides with the superconducting transition of its *largest* constituent grain. Since this is  
196 the transition temperature of a grain embedded in a *metallic* matrix, formed by the amorphous-like phase,  
197 superconductivity occurs when the pairing energy scale  $\Delta$  is greater than the Thouless energy  $E_{Th} \sim \hbar D/L^2$ ,  
198 where  $L$  is the grain diameter and  $D$  is the electronic diffusion constant [29]. In other words, the time an  
199 electron dwells on a grain before diffusing out,  $t_{Th} = \hbar/E_{Th}$ , must be longer than the time it takes to form



200 superconducting correlations,  $t_A = \hbar/\Delta$ . Taking the standard dirty-limit  $\Delta \approx \hbar D/\xi_{SC}^2$ , where  $\xi_{SC}$  is the  
 201 superconducting coherence length. This criterion of  $t_{Th} > t_A$  implies that  $T_c$  is suppressed when the grain  
 202 diameter  $L \sim \xi_{SC}$ . This mechanism is different from those found in superconducting grains embedded in  
 203 insulators, where electrons do not diffuse out of the grain and  $T_c$  is only suppressed when  $\Delta$  is on the order  
 204 of the single-particle level spacing of the grain [21].

205 In this extremal grain model, larger islands have higher  $T_c$  than smaller islands because they have  
 206 more grains and, therefore, a higher probability of having an anomalously large, high- $T_c$  grain. For the  
 207 parameters in our experiments, and given the exponential probability distribution of grain sizes, an  
 208 overwhelming fraction of the grains are smaller than the coherence length  $\xi_{SC}$ . Under these conditions, as  
 209 indicated in the Appendix, the theory of Spivak *et al* [3] yields  $T_c(L) \sim \sqrt{L - \xi_{SC}}$  when  $L$  is close to but  
 210 exceeds  $\xi_{SC}$ . If we also assume that the grain's  $T_c(L)$  should saturate at the bulk value of  $T_{c0}$  as  $L \gg \xi_{SC}$ ,  
 211 the simplest expression for  $T_c(L)$  that is consistent with these requirements is

$$T_c(L) = 0 \quad \text{for } L < \xi_{sc} \tag{1}$$

$$T_c(L) = T_c^0 \sqrt{1 - \frac{\xi_{sc}}{L}} \quad \text{for } L > \xi_{sc}$$

212 where  $T_c^0$  is the bulk transition temperature of Nb, 9.1 K, and  $\xi_{SC}$  is the Ginzburg-Landau dirty-limit  
 213 superconducting coherence length of Nb.

214 In our system, grain size has a probability distribution,  $P(L)$  where  $L$  is the grain diameter. This  
 215 distribution was determined *experimentally* as  $P(L, \beta) = \beta e^{-(\beta L)}$  with a value  $\beta = 0.24 \text{ nm}^{-1}$  according to  
 216 the TEM analysis, for one of the thin films characterized in detail. This corresponds to a mean grain  
 217 diameter,  $\beta^{-1}$ , of 4.12 nm for this value of  $\beta$ . As mentioned at the end of section A2, because what is  
 218 pertinent for our analysis is the size of individual grains, the grain size distribution extracted from TEM  
 219 data is the most relevant and is used for the theoretical analysis.

220 An island of diameter  $d$  has, on an average,  $N \sim \rho \pi d^2/4$  grains of varying sizes, where  $\rho$  is the  
 221 number density of grains. The grain density  $\rho$  depends upon two factors, the mean grain diameter  $\beta^{-1}$ , and  
 222  $f$ , the area fraction of the island that is occupied by crystalline Nb, ( $1-f$ ) being the area fraction covered by  
 223 the second amorphous-like phase. In principle, both parameters  $\beta$ , and  $f$ , can vary depending upon the

224 deposition and processing conditions such as chamber pressure, resist used, substrate temperature,  
225 technique used for Nb deposition (e-beam evaporation vs sputtering, for example), etc.

### 226 C. Simulations of extremal-grain model

227 The simulation proceeds as follows: It determines  $N$ , the expected average number of Nb grains  
228 on one island (this depends upon the island diameter  $d$ ,  $\beta$ , and  $f$ ). Then draws  $N$  grains from the  
229 distribution  $P(L, \beta) = \beta e^{-\beta L}$  and finds  $L_{\max}$ , the largest grain diameter in that set. From this the island  $T_c$  is  
230 computed using Eq. (1) with  $L = L_{\max}$ . This process was repeated for 4000 islands of the same diameter.  
231 The corresponding 4000 values of island  $T_c$  are used to compute the mean  $T_c$  and the standard deviation of  
232  $T_c$  for that particular value of island diameter. The computed results for this model are shown in Fig. 8  
233 and compared with our key experimental results.

234 Out of the three parameters introduced so far for this model ( $\xi_{\text{SC}}$ ,  $\beta$ ,  $f$ ), two are known to us with  
235 some confidence.  $\beta$ , which is related to the mean grain-size, is experimentally determined (via TEM) to  
236 be  $0.24 \text{ nm}^{-1}$ .  $\xi_{\text{SC}}$  is the Ginzburg-Landau dirty-limit superconducting coherence length of Nb, which was  
237 estimated in our previous study of arrays of Nb islands, to be approximately 29 nm [19], although it can  
238 vary depending upon the deposition conditions and the purity of the films.  $(1-f)$  is the area fraction of the  
239 island that is covered by the second amorphous-like metallic phase. So, the parameter  $f$  can, in principle,  
240 vary substantially with the kind of resist used, the deposition conditions, etc., and it can even be  
241 correlated with the island diameter; however, we find that the overall dependence of mean  $T_c$  and the  
242 standard deviation of  $T_c$  as a function of island diameter is rather weakly dependent upon the specific  
243 value of  $f$ . Although we do not have direct experimental measures on the value of  $f$  for the full range of  
244 our samples, we can place limits on the range over which it can vary by an analysis of the normal state  
245 resistance using a percolation model. Our random resistor network analysis, discussed in the next section,  
246 suggests that  $f$  is less than 0.6, which is consistent with c-AFM analysis. For the smallest islands, where  
247 interactions with the products of outgassing from PMMA can be quite large,  $f$  could be smaller.  
248 Simulations indicated by black points in Fig. 8(a) and Fig. 8(c), and labeled by  $S = 9.1 \text{ K}$ , correspond to  
249 this particular constrained case, with  $\beta = 0.24 \text{ nm}^{-1}$ ,  $\xi_{\text{SC}} = 29 \text{ nm}$ , and values of  $f$  that are correlated with  
250 the island diameter (smaller area fraction of Nb grains for smaller diameters.)

251 We note that simulation results for this constrained case are in semi-quantitative agreement with  
 252 the major aspects of the observed results. The overall shape of the observed behavior of mean  $T_c$  as a  
 253 function of island diameter, is captured correctly by the simulations. This includes the suppression of  $T_c$   
 254 below 1400 nm and the saturation of  $T_c$  at large diameters. As shown in Fig. 8(c), the experimentally  
 255 observed increase of standard deviation of  $T_c$  for smaller values of mean  $T_c$  is correctly predicted by the  
 256 model, as is the approximate magnitude of these island-to-island variations in  $T_c$ .

257 Even though this constrained model accounts for key features of the data, it is clear from Fig. 8  
 258 that the computed results show deviations from the experimental results. We thus consider the effects of  
 259 varying parameters to obtain better agreement. A straightforward variant is to assume that grain  $T_c(L)$   
 260 increases much more rapidly for  $L > \xi_{sc}$ , but it does not exceed the bulk value of  $T_c$ . Thus, we can  
 261 normalize by a factor  $S$  rather than by 9.1 K as shown in Eq. (2).

$$T_c(L) = 0 \quad \text{for } L < \xi_{sc} \quad (2)$$

$$T_c(L) = \text{Min} \left[ 9.1, S \sqrt{1 - \frac{\xi_{sc}}{L}} \right] \quad \text{for } L > \xi_{sc}$$

262 The effect of varying the  $S$  parameter is indicated in Fig. 8(b). Increasing  $S$  has the effect of  
 263 narrowing the window of grain diameters that will produce a  $T_c$  between 0 K and 9.1 K. For  $S = 12$  K, the  
 264 grain sizes playing a role in the transition are between 29 nm and 45 nm as shown in Fig. 8(b). At larger  
 265 grain diameters, the grain  $T_c$  saturates to the bulk value of 9.1 K, as one would expect. Stated differently,  
 266 this corresponds to the assumption that grains above 45 nm diameter have an onset  $T_c$  that equals the bulk  
 267  $T_c$ , possibly because they experience additional proximity coupling. The traces labelled  $S = 12$  K in Fig. 8  
 268 show the simulation results (red points) based upon Eq. (2). While this gives a much better agreement for  
 269 the numerical values of mean  $T_c$ , and for the overall trend of  $T_c$  as a function of diameter, than that  
 270 predicted by  $S = 9.1$  K, the agreement with the observed behavior of standard deviation of  $T_c$  versus the  
 271 corresponding mean value of  $T_c$  is worse.

272 One can consider all four parameters of the model ( $\xi_{sc}$ ,  $\beta$ ,  $S$ ,  $f$ ) as being adjustable, to some  
 273 extent, and explore if that might yield simultaneous agreement with all aspects of the data. It might also  
 274 provide an explanation for the dependence of the trends upon deposition conditions (for example, quality  
 275 of the chamber vacuum, deposition technique, resist used).

- 276 (1)  $\beta$ , which is related to the mean grain-size, can, in principle, depend upon deposition conditions.  
277 But the computed results are extremely sensitive to the value of  $\beta$  and changing  $\beta$  significantly  
278 away from the experimentally determined value of  $0.24 \text{ nm}^{-1}$  results in worse agreement with  
279 data. Therefore, varying  $\beta$  cannot explain all the observed variations from one deposition to  
280 another.
- 281 (2) Varying  $S$  changes the computed results in a systematic way, as indicated in Fig. 8 and it does  
282 help in improving agreement with some aspects (particularly the experimental saturation of  $T_c \sim$   
283  $9\text{K}$ ), but at the expense of some other aspects such as the standard deviation.
- 284 (3) Varying  $\xi_{\text{sc}}$  for different diameters is not especially meaningful, given that the Nb purity is  
285 unlikely to vary much across a chip, and this too does not improve the agreement with theory  
286 significantly.
- 287 (4) For the smallest islands, where interactions with the products of outgassing from PMMA can be  
288 quite large,  $f$  can be quite small. Thus, one can assume values of  $f$  that are correlated with the  
289 diameter, i.e. smaller area fraction of Nb grains for smaller diameters. In fact, the black and red  
290 points in Fig 8 correspond to this additional assumption.

291 Based upon simultaneous variations of these parameters within reasonable ranges, we conclude that while  
292 the extremal grain model best explains many important aspects of our data, there are remaining  
293 disagreements that deserve further study.

294 Overall, the anomalous size-dependence of  $T_c$  we observe in our islands of granular Nb-films is  
295 explained semi-quantitatively as a rare-region effect: specifically, by a model in which the onset of  
296 superconductivity on an island coincides with the transition temperature of its largest constituent grain.  
297 This “extremal-grain” model both accounts for the size-dependence of the transition temperature and  
298 predicts variations in  $T_c$  for islands of fixed size. Thus, we provide evidence for rare-region effects in a  
299 system having  $R \ll R_Q$ .

### 300 ***1. Alternative Models and Random Resistor Network Simulation***

301 While the extremal grain model does agree with much of our data, as discussed above, it is  
302 important to rule out alternative explanations, particularly because the island normal state resistance,  $R_N$ ,  
303 also scales with island diameter [Fig. 9(c)].

304 We first consider the role of shunting resistance and normal metal suppression from the contacts  
305 by measuring Nb islands having underlying Au films, which provide a resistive shunt across the island  
306 and greater normal metal suppression. As can be seen E2 Au of Fig. 2, the  $T_c$ 's of islands with underlying  
307 Au were similar to those of islands without underlying Au, indicating that neither suppression from  
308 normal metal contacts nor shunting resistance significantly altered  $T_c$ .

309 The dependence of island normal state resistance on island diameter can be best explained by  
310 transport through a highly granular material, where most of the current passes through the most  
311 conducting paths. Since fewer of these highly conductive paths are available for small diameter islands,  
312 both the mean value and the variation in  $R_N$  is greater for smaller diameter islands [Fig 9(c) and 9(d)]. We  
313 provide the results of a simulation that uses a random percolating network [30,31,32] to explain, semi-  
314 quantitatively, our data for the dependence of island normal state resistance on island diameter.

315 Tuning the probability of a connection between adjacent nodes existing,  $p$ , and a connection not  
316 existing,  $1-p$ , the random network studies observe a phase transition at a critical probability,  $p_c$ , from  
317 finite sized clusters for  $p < p_c$  to an infinite cluster of linked nodes throughout the network for  $p > p_c$ . The  
318 relevant length scale involved is the correlation length,  $\xi \propto |p-p_c|^{-\alpha}$ , where  $\alpha$  is a scaling constant. This  
319 corresponds to the radius of the largest percolative clusters for  $p < p_c$  and the radius of the largest holes in  
320 the infinite percolative cluster in  $p > p_c$ .

321 Our system corresponds more closely to the case of a good conductor in a poor conductor, which  
322 can be studied by giving the open links a large but finite resistance [33]. The resistance of this can be seen  
323 in Fig. 9(a), with a crossover near  $p_c \sim 0.6$ . For  $p < p_c$ , sample resistance is dominated by weak links  
324 between network clusters, and for  $p > p_c$ , the conductance is dominated by a single spanning cluster. The  
325 finite size behavior of this model results in either a network cluster spanning the array or a hole in a  
326 network cluster dividing the array. This leads to array resistance distribution splitting as the array width,  
327  $L$ , decreases. This splitting is shown on a logarithmic scale in Fig. 9(b) for a specific value of  $p = 0.55$ .  
328 Due to proximity of this  $p$  to  $p_c$ , the upper and lower curves are approximately equal in magnitude, but the  
329 lower curve is suppressed for  $p < p_c$  and the upper curve is suppressed for  $p > p_c$ .

330 Since we observe increasing resistance with decreasing island diameters, our data Fig. 9(c)  
331 corresponds to the  $p < p_c$  case involving weakly linked network clusters. The relevant length scale of this  
332 system is the spacing of key current paths, which corresponds to the size of a low resistance network-

333 cluster. This does not correspond to a single Nb grain, which would yield finite size effects on the scale of  
334 nanometers. Instead, the network-cluster likely corresponds to clusters of grains, and that is qualitatively  
335 consistent with both the large increase in  $R_N$  [Fig. 9(c)], and also the large island-to-island fluctuations of  
336  $R_N$  [Fig 9(d)] below diameters of approximately 700 nm.

## 337 V. CONCLUSIONS

338 Our results suggest a particular physical picture of the local nature of the superconducting state  
339 near the superconductor-metal transition in this system: this state is inhomogeneous and is dominated by  
340 rare-regions, as suggested in Refs. [3,34]. By exploring micron-scale systems, and by carefully correlating  
341 microstructure with modelling, we have been able to show the influence of rare-regions on  
342 superconducting transport. We have found, remarkably, that even when grains are coupled strongly  
343 enough that the normal-state resistance is small, the superconducting transition can still be captured via a  
344 model of effectively decoupled “grains.” In this sense, our micron-scale superconducting islands behave  
345 like many other strongly random quantum systems, such as high-temperature superconductors [35,36].  
346 We note that the “rare-region” effects we have discussed are not limited to granular Nb and should appear  
347 in other disordered systems of superconducting puddles within a *metallic* matrix.

## 348 ACKNOWLEDGEMENTS

349 We thank Vadim Oganessian and Aharon Kapitulnik for helpful discussions. We also thank  
350 Mauro Sardela and James Lee for performing the XRD measurements and analysis, Scott Maclaren for  
351 assistance with conducting AFM and Timothy Spila for performing the RBS measurements. This work  
352 was supported by the DOE Basic Energy Sciences under DE-SC0012649 and the National Science  
353 Foundation (NSF) under DMR 17-10437. SG acknowledges funding from the Walter Burke Institute. JK  
354 and JMZ are supported as part of the Center for Emergent Superconductivity, an Energy Frontier  
355 Research Center funded by the US Department of Energy, Office of Science, Office of Basic Energy  
356 Sciences, under award number DE-AC0298CH10886. This research was carried out in part in  
357 the Frederick Seitz Materials Research Laboratory Central Research Facilities at the University of Illinois.

## 358 APPENDIX

359 We begin with the Landau free energy for a single superconducting grain in a metallic matrix Eq.  
360 (1) of Spivak et al [3].

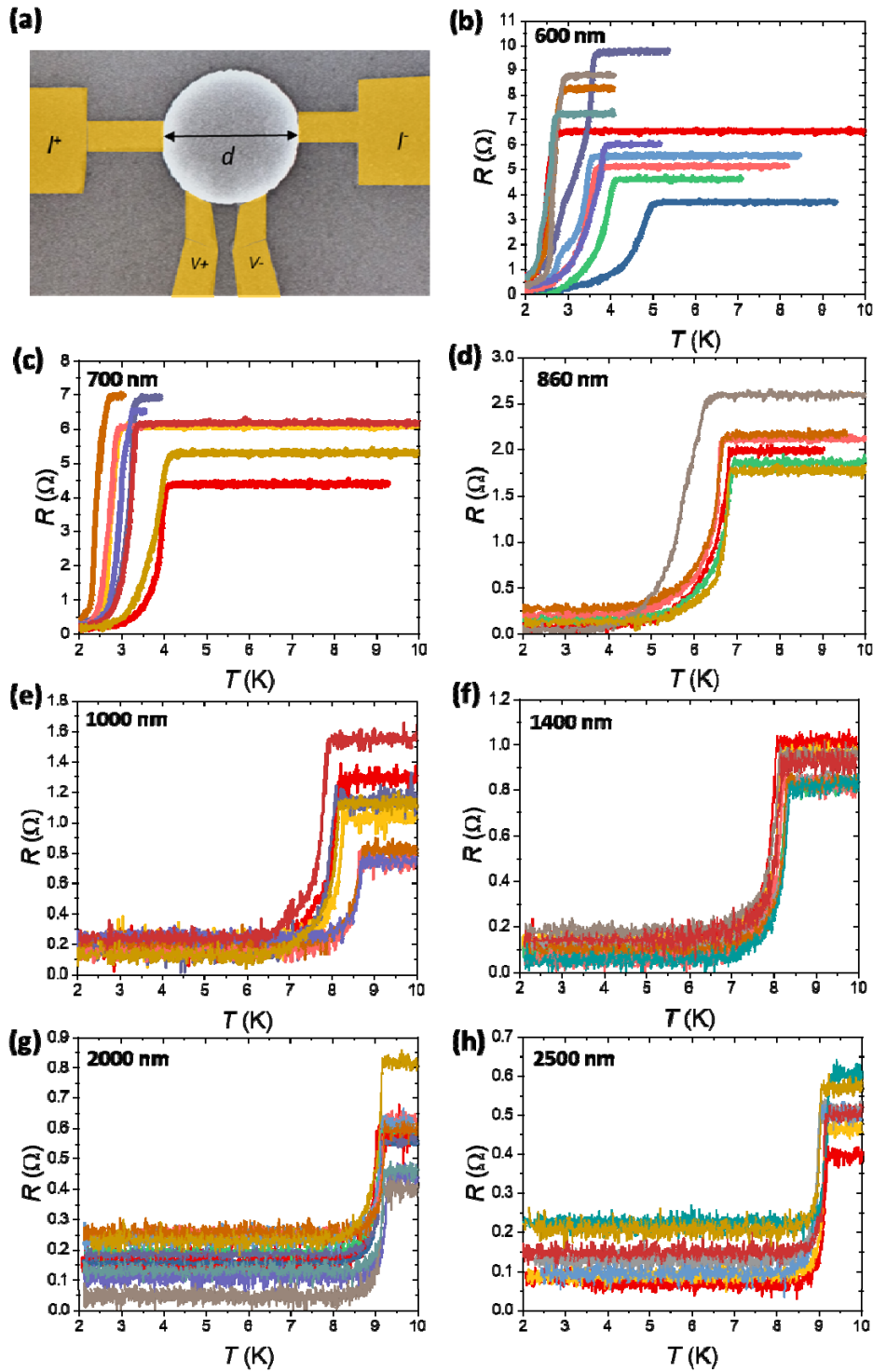
$$F = -\frac{(\gamma - \gamma_c)\Delta^2}{2} + \frac{\Delta^4}{4\Delta_0^2} + \dots$$

361 For simplicity (and to avoid subtleties specific to the zero-temperature limit) we assume that the system is  
362 at some nonzero temperature that is much lower than the bulk  $T_c$ . The control parameter  $\gamma$  depends on the  
363 size of the grain  $L$ , because the proximity effect from neighboring metallic grains suppresses  
364 superconducting fluctuations on the anomalously large grain. The extent of this suppression depends in a  
365 complicated way on the size of the grain and the properties of the metallic grains, oxide layers, etc. [De  
366 Gennes, RMP 36, 225 (1964)]. For  $\gamma$  near the critical value  $\gamma_c$ , we can Taylor-expand the  $L$ -dependence  
367 to linear order, giving the Landau free energy

$$F = -\frac{c(L - L_c)\Delta^2}{2} + \frac{\Delta^4}{4\Delta_0^2}$$

368 for some constant  $c$ . Minimizing this free energy gives the result in the main text.

369



370

FIG.1. Representative scanning electron microscope (SEM) device image and island-to-island fluctuations of  $T_c$  for various island diameters. (a) False color SEM image of island and leads (yellow) where  $d$  is island diameter. Resistance versus temperature data for island diameters of (b) 600nm, (c) 700 nm, (d) 860 nm, (e) 1000 nm, (f) 1400 nm, (g) 2000 nm and (h) 2500 nm. Each  $R(T)$  panel contains temperature sweeps for 8-12 island devices.



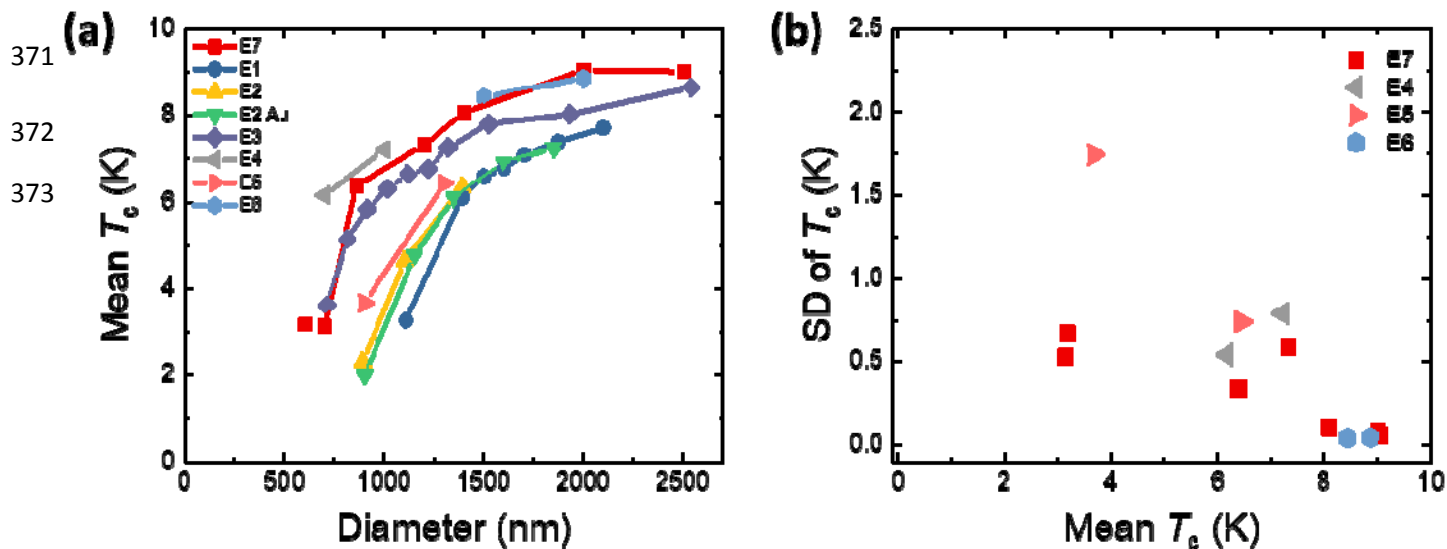


FIG. 2. Superconducting transition for different island sizes across various evaporation runs. (a) Mean  $T_c$  as a function of Island Diameter. Different colors denote different Nb evaporation runs. Each evaporation run evaluated measurements of 5 to 12 islands of the same diameter (except for E1-E3 where only one island per diameter was evaluated). The samples indicated by E2 Au have underlying Au. E3 was obtained using a lower evaporation pressure. (b) Standard deviation of the island-to-island variation of  $T_c$  for evaporations 4-7 (E4-E7).

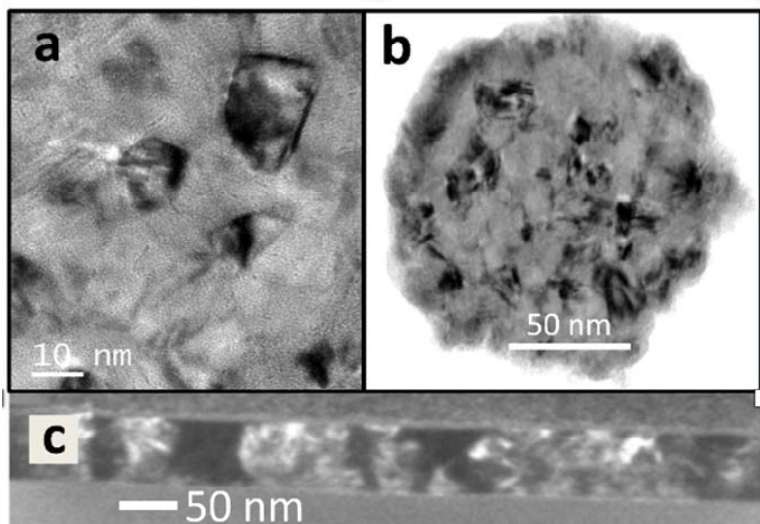


FIG. 3. TEM images showing film morphology. (a) Zoomed in TEM image showing crystalline Nb grains in black and an amorphous-like metallic phase of Nb in gray. (b) TEM of a 130 nm diameter Nb island. TEM images in (a) and (b) were performed on 30 nm thick Nb. (c) Cross-sectional TEM (dark field) performed on 70 nm thick Nb showing columnar grains.

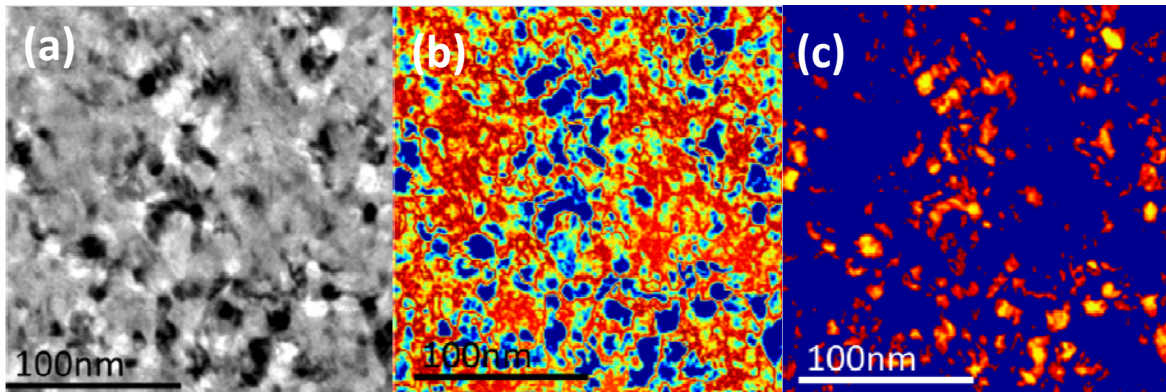


FIG. 4. TEM image processing used to extract grain size distribution. (a) A raw TEM image of a Nb film. High contrast grains are visible in both black and white. (b) The TEM image after a low pass filter has been applied, mean intensity is subtracted, and the absolute value is taken. High contrast grains appear in blue. (c) The high contrast grains identified by the object finder are shown in red and orange.

374

375

376

377

378

379

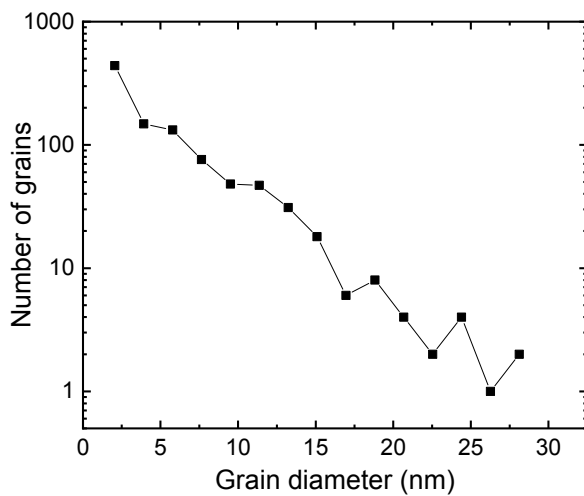
380

381

382

383

384



385

386

387

388

389

390

FIG. 5. TEM grain size distribution. Histogram of Nb grains extracted using TEM demonstrating an exponential distribution of grains. The fitted mean grain diameter is 4.12 nm.

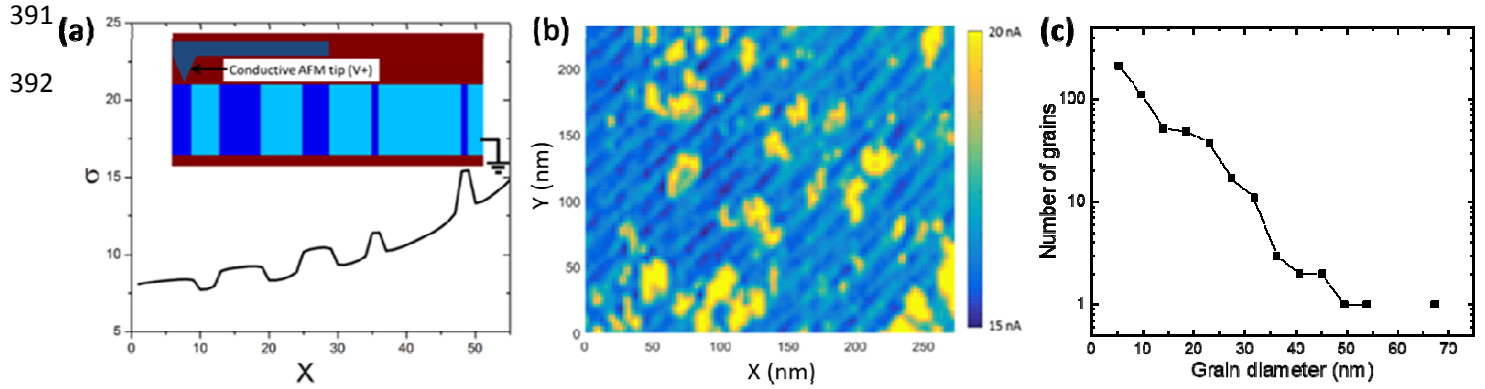


FIG. 6. Conductive AFM and its use to extract grain size distribution. (a) Inset shows a model granular film with columnar features similar to those observed in our system. Blue corresponds to low resistances, light blue corresponds to intermediate resistances 3 times higher, and red corresponds to insulating. The plot shows simulated conductance as the tip is dragged along these features. (b) A conductive AFM measurement of a Nb film with fixed bias voltage. Current peaks are visible with width comparable to that of the grains. (c) Histogram of conductive AFM grains extracted with an object finder. The fitted mean grain diameter is 8.2 nm.

393  
394  
395  
396  
397  
398  
399  
400  
401  
402  
403  
404  
405  
406

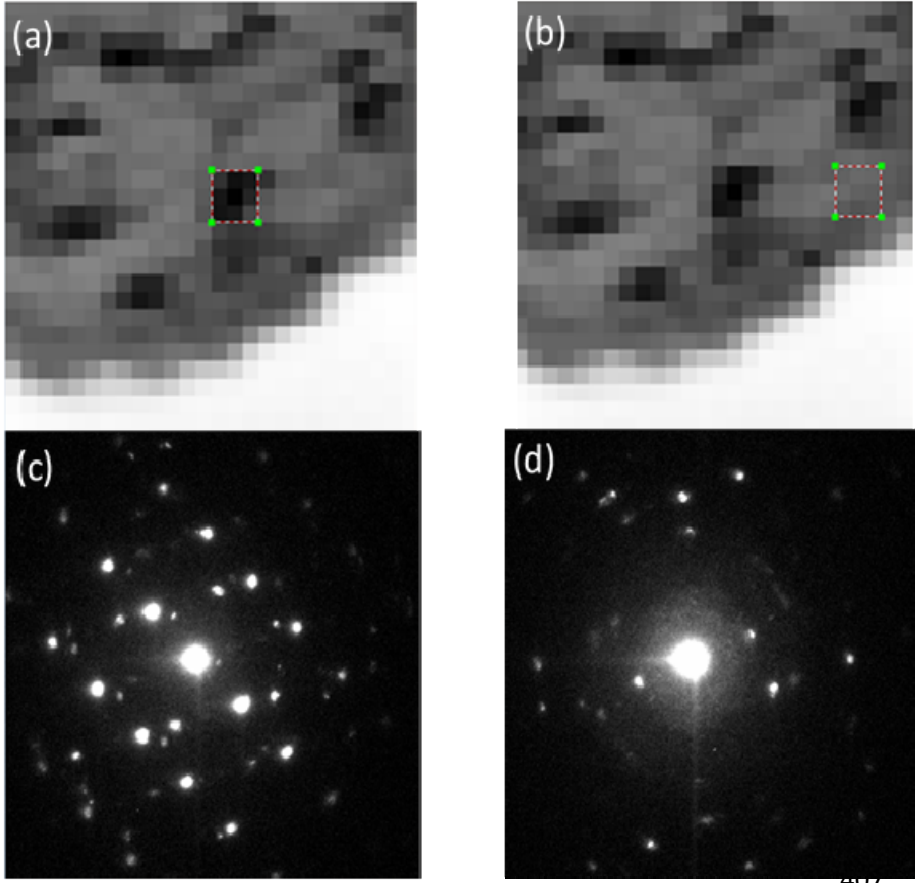


FIG. 7. Virtual bright-field TEM images and Selective Area Diffraction patterns. (a) and (b) show a virtual bright-field TEM image of a 104 nm square region of a Nb island obtained using scanning electron nanodiffraction with a step size of 4 nm [28], with two different selected areas identified by nine-pixel squares (12 nm by 12 nm) in each case. (c) and (d) show the diffraction patterns from the two corresponding areas (a) and (b) respectively. (c) Shows the sharp diffraction spots, corresponding to highly crystalline Nb in the dark grains. (d) Shows a combination of a diffuse halo, a signature of an amorphous component, and some spots corresponding to a nano-crystalline/amorphous phase.

409  
410  
411  
412  
413

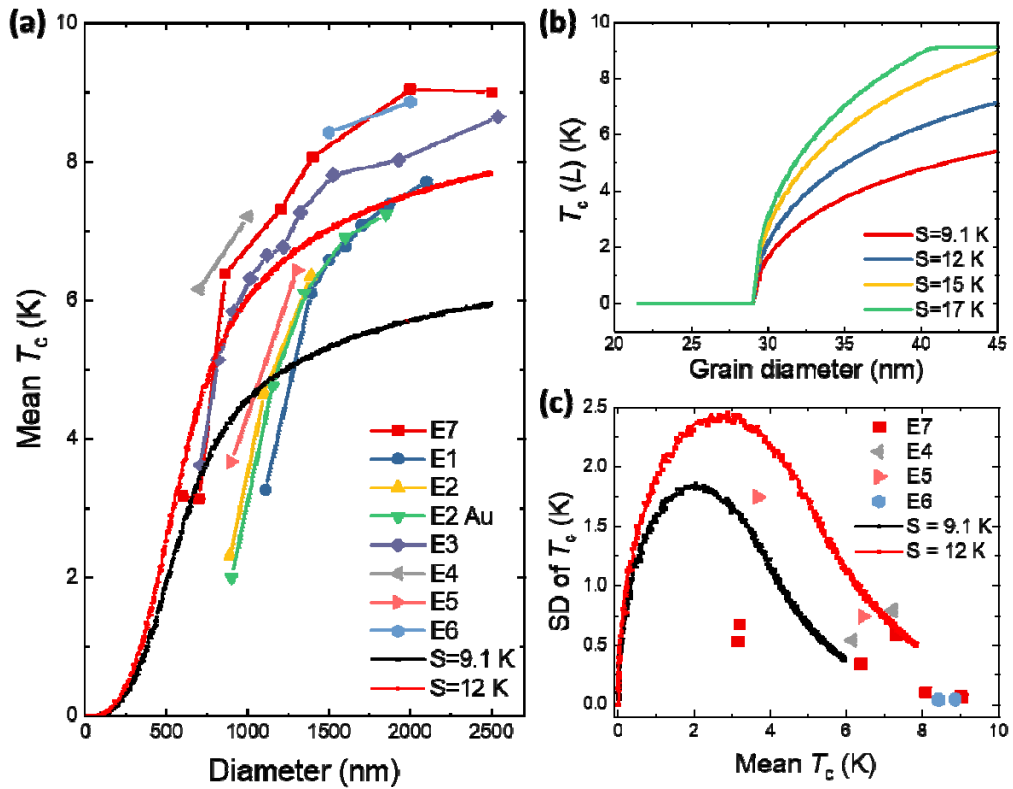
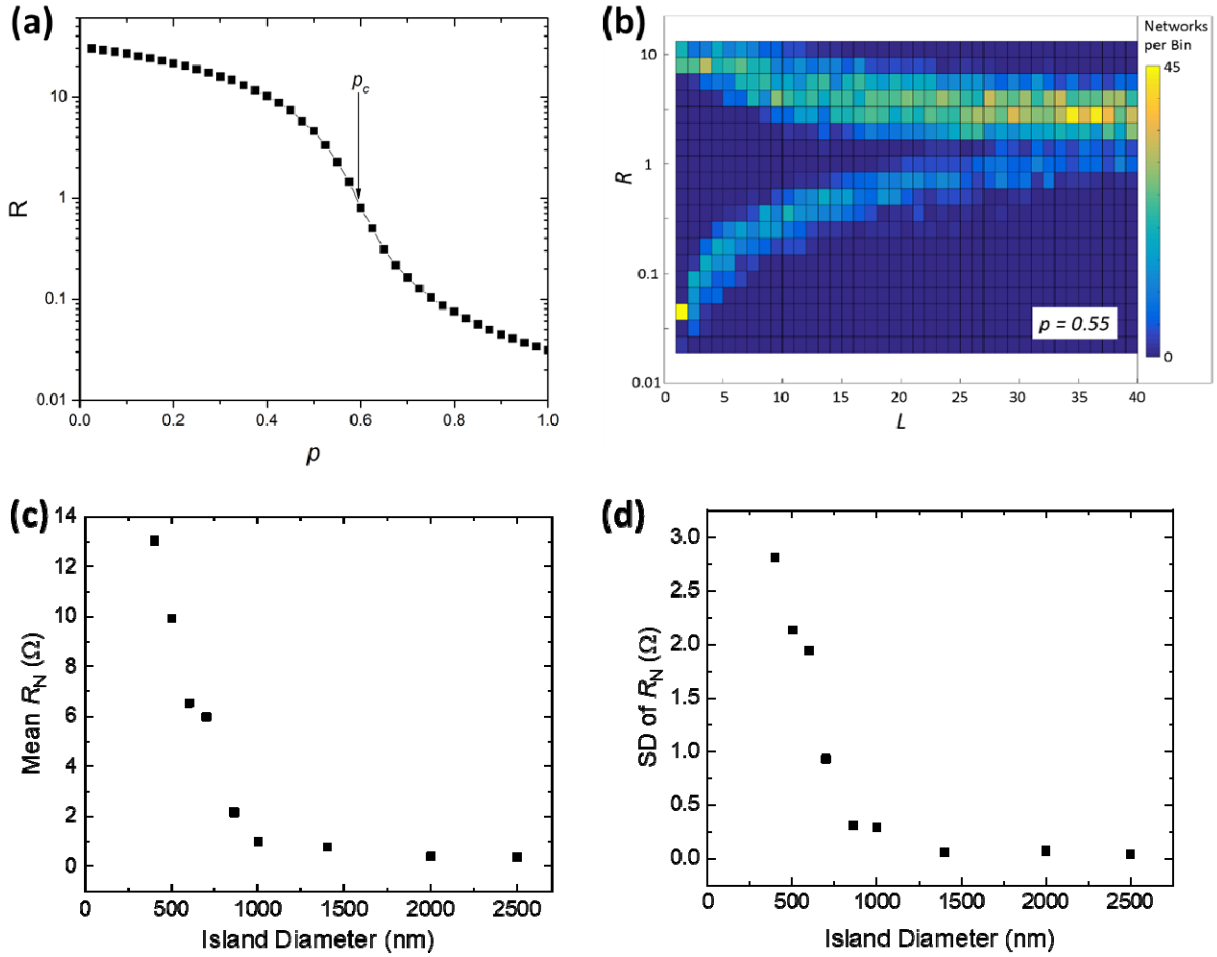


FIG. 8. Extremal-Grain Model. (a) The simulated grain sizes are applied to Eq. 2 to obtain an estimate of  $T_c$  as a function of island diameter. Mean simulated  $T_c$  for two  $S$  values (black and red curves) is shown alongside data from evaporations 1-7 (E1-E7). (b) Grain critical temperature  $T_c(L)$  as a function of grain diameter as  $S$  is varied in Eq. 2. (c) Simulated standard deviation as a function of mean  $T_c$  for the two same  $S$  values (black and red) shown alongside evaporations 4-7 (E4-E7).



415

FIG. 9. Simulations of Random Network of Resistors. (a) The resistance of a random resistor model with a probability,  $p$ , of there being a low resistance connection rather than a high resistance connection. (b) A histogram of resistance as a function of  $L$ , the width of a square array. The islands split into two groupings with increasing  $L$ , one with lower resistance that is spanned by a low resistance network, and another that is split by a hole in the network. The two groupings are equal in number near  $p_c$ , but the higher resistance grouping is dominant for  $p < p_c$  and the lower resistance grouping dominates  $p > p_c$ . (c) Our data for mean  $R_N$  vs. island diameter for evaporation 7 (E7), clearly corresponds to the  $p < p_c$  case involving weakly linked network clusters. (d) Island to island fluctuations of  $R_N$  increase rapidly below  $\sim 700$  nm, which is consistent (see text) with our random resistor network model for  $p < p_c$ .

416

417

- 
- <sup>1</sup> E. Miranda, V. Dobrosavljevic, Disorder-driven non-Fermi liquid behavior of correlated electrons. *Rep. Prog. Phys.* **68**, 2337 (2005).
- <sup>2</sup> D. S. Fisher, Phase Transitions and Singularities in Random Quantum systems. *Physica A.* **263**, 222 (1999).
- <sup>3</sup> B. Spivak, P. Oreto, S. A. Kivelson, Theory of quantum metal to superconductor transitions in highly conducting systems. *Phys. Rev. B* **77**, 214523 (2008).
- <sup>4</sup> D. Kowal, Z. Ovadyahu, Scale dependent superconductor-insulator transition. *Physica C.* **468**, 322 (2008).
- <sup>5</sup> M. V. Feigel'man, A. I. Larkin, M. A. Skvortsov, Quantum Superconductor-Metal transition in a Proximity Array. *Phys. Rev. Lett.* **86**, 1869 (2001).
- <sup>6</sup> B. Sacépé, C. Chapelier, T. I. Baturina, V. M. Vinokur, M. R. Baklanov, M. Sanquer, Disorder-Induced Inhomogeneities of the Superconducting State Close to the Superconductor-Insulator Transition. *Phys. Rev. Lett.* **101**, 157006 (2008).
- <sup>7</sup> Y. Xing, H.-M. Zhang, H.-L. Fu, H. Liu, Y. Sun, J.-P. Peng, F. Wang, X. Lin, X.-C. Ma, Q.-K. Xue, J. Wang, and X. C. Xie, Quantum Griffiths singularity of superconductor-metal transition in Ga thin films. *Science* **350**, 542 (2015).
- <sup>8</sup> L. Zhao, H. Deng, I. Korzhovska, M. Begliarbekov, Z. Chen, E. Andrade, E. Rosenthal, A. Pasupathy, V. Oganessian, and L. Krusin-Elbaum, Emergent surface superconductivity in the topological insulator  $\text{Sb}_2\text{Te}_3$ . *Nature Comm.* **6**, 8279 (2015).
- <sup>9</sup> J. Biscaras N. Bergeal, S. Hurand, C. Feuillet-Palma, A. Rastogi, R. C. Budhani, M. Grilli, S. Caprara, J. Lesueur, Multiple quantum criticality in a two-dimensional superconductor. *Nat. Mater.* **12**, 542 (2013).
- <sup>10</sup> F.M. Izrailev, A.A. Krokhnin, N.M. Makarov, Anomalous localization in low-dimensional systems with correlated disorder, *Physics Reports* **512**, 125 (2012).
- <sup>11</sup> N. Mason, A. Kapitulnik, Dissipation Effects on the Superconductor-Insulator Transition in 2D Superconductors. *Phys. Rev. Lett.* **82**, 5341 (1999).
- <sup>12</sup> M. P. A. Fisher, Dissipation and quantum fluctuations in granular superconductivity, *Phys. Rev. B* **36**, 1917 (1987).
- <sup>13</sup> H. M. Jaeger, D. B. Haviland, B. G. Orr, A. M. Goldman, Onset of superconductivity in ultrathin granular metal films. *Phys. Rev. B* **40**, 182 (1989).
- <sup>14</sup> Y. Saito, Y. Kasahara, J. Ye, Y. Iwasa, T. Nojima, Metallic ground state in an ion-gated two-dimensional superconductor. *Science* **350**, 409 (2015).
- <sup>15</sup> G. Deutscher, O. Entin-Wohlman, S. Fishman, Y. Shapira, Percolation description of granular superconductors, *Phys. Rev. B* **21**, 5041 (1980).
- <sup>16</sup> O. Entin-Wohlman, A. Kapitulnik, Y. Shapira, Dependence of  $T_c$  on the normal-state resistivity in granular superconductors, *Phys. Rev. B* **24**, 6464 (1981).
- <sup>17</sup> Z. Han, A. Allain, H. Arjmandi-Tash, K. Tikhonov, M. Feigel'man, B. Sacépé, V. Bouchiat, Collapse of superconductivity in a hybrid tin-graphene Josephson junction array. *Nat. Phys.* **10**, 380 (2014).
- <sup>18</sup> A. Kamlapure, T. Das, S. C. Ganguli, J. B. Parmar, S. Bhattacharyya, P. Raychaudhuri, Emergence of nanoscale inhomogeneity in the superconducting state of a homogeneously disordered conventional superconductor, *Scientific Reports* **3**, 2979 (2013)
- <sup>19</sup> S. Eley, S. Gopalakrishnan, P. M. Goldbart, N. Mason, Approaching zero-temperature metallic states in mesoscopic superconductor-normal-superconductor arrays. *Nat. Phys.* **8**, 59 (2012).
- <sup>20</sup> P. □ W. Anderson, Theory of dirty superconductors. *J. Phys. Chem. Solids* **11**, 26 (1959).
- <sup>21</sup> D. C. Ralph, C. T. Black, M. Tinkham, Spectroscopic Measurements of Discrete Electronic States in Single Metal Particles. *Phys. Rev. Lett.* **74**, 3241 (1995).

- 
- <sup>22</sup> S. Bose, A.M. García-García, M. M. Ugeda, J. D. Urbina, C. H. Michaelis, I. Brihuega, K. Kern, Observation of shell effects in superconducting nanoparticles of Sn. *Nat. Mater.* **9**, 550 (2010).
- <sup>23</sup> W.-H. Li, C. C. Yang, F. C. Tsao, K. C. Lee, Quantum size effects on the superconducting parameters of zero-dimensional Pb nanoparticles. *Phys. Rev. B* **68**, 184507 (2003).
- <sup>24</sup> S. Bose, P. Raychaudhuri, R. Banerjee, P. Vasa, P. Ayyub, Mechanism of the Size Dependence of the Superconducting Transition of Nanostructured Nb. *Phys. Rev. Lett.* **95**, 147003 (2005).
- <sup>25</sup> T. Hoss, C. Strunk, and C. Schonenberger, Non-organic evaporation mask for superconducting nano-devices, *Microelectronic Engineering* **46**, 149 (1999).
- <sup>26</sup> K. Ohnishi, T. Kimura and Y. Otani, Improvement of Superconductive Properties of Mesoscopic Nb Wires by Ti Passivation Layers, *Appl. Phys. Express* **1**, 021701 (2008).
- <sup>27</sup> Holger Bartolf, Fluctuation Mechanisms in Superconductors: Nanowire Single-Photon Counters, Enabled by Effective Top-Down Manufacturing, publisher: *Springer* (2016).
- <sup>28</sup> K. H. Kim, H. Xing, J. M. Zuo, P. Zhang, H. F. Wang, TEM based high resolution and low-dose scanning electron nanodiffraction technique for nanostructure imaging and analysis. *Micron* **71**, 39 (2015).
- <sup>29</sup> P. Dubos, H. Courtois, B. Pannetier, F. K. Wilhelm, A. D. Zaikin, G. Schön, Josephson critical current in a long mesoscopic S-N-S Junction. *Phys. Rev. B* **63**, 064502 (2001).
- <sup>30</sup> A. Miller and E. Abrahams, Impurity Conduction at Low Concentrations. *Phys. Rev.* **120**, 745 (1960).
- <sup>31</sup> V. Ambegaokar, B. I. Halperin, and J. S. Langer, Hopping Conductivity in Disordered Systems. *Phys. Rev. B* **4**, 2612 (1971).
- <sup>32</sup> D. Stauffer, Scaling theory of percolation clusters. *Phys. Rep.* **54**, 1 (1979).
- <sup>33</sup> J. Bernasconi, Real-space renormalization of bond-disordered conductance lattices. *Phys. Rev. B* **18**, 2185 (1978).
- <sup>34</sup> D. Kowal, Z. Ovadyahu, Disorder induced granularity in an amorphous superconductor. *Sol. St. Comm.* **90**, 783 (1994).
- <sup>35</sup> A. N. Pasupathy, A. Pushp, K. K. Gomes, C. V. Parker, J. Wen, Z. Xu, G. Gu, S. Ono, Y. Ando, A. Yazdani, Electronic Origin of Inhomogeneous Pairing Interaction in the High- $T_c$  Superconductor  $\text{Bi}_2\text{Sr}_2\text{CaCu}_2\text{O}_{8+\delta}$ . *Science* **320**, 196 (2008).
- <sup>36</sup> K. K. Gomes, A. N. Pasupathy, A. Pushp, S. Ono, Y. Ando, A. Yazdani, Visualizing pair formation on the atomic scale in high- $T_c$  superconductor  $\text{Bi}_2\text{Sr}_2\text{CaCu}_2\text{O}_{8+\delta}$ . *Nature* **447**, 569 (2007).